HemaSphere

ARTICLE

Activating mutations remodel the chromatin accessibility landscape to drive distinct regulatory networks in *KMT2A*-rearranged acute leukemia

Qirui Zhang[1,^] | Ton Falqués-Costa[1,^] | Mattias Pilheden[1] | Helena Sturesson[1] | Tina Ovlund[1] | Vendela Rissler[1] | Anders Castor[2] | Hanne V. H. Marquart[3,4] | Birgitte Lausen[5] | Thoas Fioretos[1] | Axel Hyrenius-Wittsten[1] | Anna K. Hagström-Andersson[1]

Correspondence: Anna K. Hagström-Andersson (Anna.Hagstrom@med.lu.se)

Abstract

Activating *FLT3* and *RAS* mutations commonly occur in leukemia with *KMT2A*-gene rearrangements (*KMT2A*-r). However, how these mutations cooperate with the *KMT2A*-r to remodel the epigenetic landscape is unknown. Using a retroviral acute myeloid leukemia (AML) mouse model driven by *KMT2A::MLLT3*, we show that *FLT3^ITD^*, *FLT3^N676K^*, and *NRAS^G12D^* remodeled the chromatin accessibility landscape and associated transcriptional networks. Although the activating mutations shared a common core of chromatin changes, each mutation exhibits unique profiles with most opened peaks associating with enhancers in intronic or intergenic regions. Specifically, *FLT3^N676K^* and *NRAS^G12D^* rewired similar chromatin and transcriptional networks, distinct from those mediated by *FLT3^ITD^*. Motif analysis uncovered a role for the AP-1 family of transcription factors in *KMT2A::MLLT3* leukemia with *FLT3^N676K^* and *NRAS^G12D^*, whereas Runx1 and Stat5a/Stat5b were active in the presence of *FLT3^ITD^*. Furthermore, transcriptional programs linked to immune cell regulation were activated in *KMT2A*-r AML expressing *NRAS^G12D^* or *FLT3^N676K^*, and the expression of NKG2D-ligands on *KMT2A*-r cells rendered them sensitive to CAR T cell-mediated killing. Human *KMT2A*-r AML cells could be pharmacologically sensitized to NKG2D-CAR T cells by treatment with the histone deacetylase inhibitor LBH589 (panobinostat) which caused upregulation of NKG2D-ligand levels. Co-treatment with LBH589 and NKG2D-CAR T cells enabled robust AML cell killing, and the strongest effect was observed for cells expressing *NRAS^G12D^*. Finally, the results were validated and extended to acute leukemia in infancy. Combined, activating mutations induced mutation-specific changes in the epigenetic landscape, leading to changes in transcriptional programs orchestrated by specific transcription factor networks.

INTRODUCTION

Genetic rearrangements of the *lysine methyltransferase 2A* gene (*KMT2A*-r, previously *MLL*) are seen in around 10% of acute leukemia.[1] Infant acute lymphoblastic leukemia (ALL) is characterized by *KMT2A*-r in around 80% of cases and is associated with a poor outcome.[2] However, newer treatments including blinatumomab or chimeric antigen receptor (CAR) T cell therapy may change this poor outcome.[3,4]

We and others have shown that infant *KMT2A*-r ALL has a mutationally silent genome.[5,6] Despite the paucity of mutations, activating kinase or PI3K/RAS-pathway mutations were observed in half of the cases. Further, in infants with *KMT2A::AFF1*, the presence of an activating mutation is associated with an average younger age at diagnosis, suggesting that they accelerate the disease.[6] In agreement, using a retroviral acute myeloid leukemia (AML) mouse model, we showed that co-expression of *KMT2A::MLLT3* with *FLT3^ITD^*, *FLT3^N676K^* or *NRAS^G12D^* accelerated disease onset and caused specific gene expression profiles.[7]

[1]Department of Laboratory Medicine, Division of Clinical Genetics, Lund University, Lund, Sweden

[2]Childhood Cancer Center, Skåne University Hospital, Lund, Sweden

[3]Department of Clinical Immunology, National University Hospital, Rigshospitalet, Copenhagen, Denmark

[4]Department of Clinical Medicine, Faculty of Health and Medical Sciences, University of Copenhagen, Copenhagen, Denmark

[5]Department of Paediatrics and Adolescent Medicine, Rigshospitalet, University of Copenhagen, Copenhagen, Denmark

^These authors contributed equally to this work.

Accessible chromatin is essential for transcription factor (TF) binding, and AML with different genetic alterations has been shown to adopt subtype-specific chromatin accessibility landscapes that are associated with certain transcription factors and regulatory networks.[8] However, how activating mutations rewire the chromatin accessibility landscape and TF binding sites to drive gene expression programs in KMT2A-r acute leukemia is unknown. To address this, we used the Assay for Transposase-Accessible Chromatin using sequencing (ATAC-seq)[9] and RNA-sequencing to study murine leukemia transformed with KMT2A::MLLT3-alone or together with FLT3^{ITD}, FLT3^{N676K}, or NRAS^{G12D}, all common activating mutations in human leukemia. To extend the results to human leukemia, we analyzed five infant KMT2A-r acute leukemia cases with and without activating mutations. Our data demonstrate mutation-specific changes in the epigenetic landscape with most newly opened chromatin peaks overlapping with putative enhancers in intronic/intergenic regions, which might function to drive specific gene expression programs. FLT3^{N676K} and NRAS^{G12D} rewired similar transcriptional networks, and motif analysis revealed a role of the AP-1 family of TFs, whereas Runx1 and Stat5a/Stat5b were active in the presence of FLT3^{ITD}. Further, immune activity transcriptional programs were enhanced by NRAS^{G12D} and FLT3^{N676K}. The expression of NKG2D-ligands on the KMT2A-r cells rendered them sensitive to CAR T cell-mediated killing. Finally, the results were validated and extended to acute leukemia in infancy, showing an overlap in how activating mutations promote leukemogenesis.

METHODS

Mouse model and patient samples

We studied leukemia bone marrow (BM) from mice with KMT2A::MLLT3 and either FLT3^{ITD}, FLT3^{N676K}, NRAS^{G12D}, or empty vector (n = 4 per genotype) (Supporting Information S1: Table 1).[7] Briefly, mice were transplanted with cells transduced with either MSCV-KMT2A::MLLT3-IRES-mCherry and MSCV-FLT3^{ITD}-IRES-GFP, MSCV-FLT3^{N676K}-IRES-GFP, MSCV-NRAS^{G12D}-IRES-eGFP or MSCV-IRES-eGFP. Details on the mice are given in Hyrenius-Wittsten et al., Nat Commun 2018.[7] In brief, mice develop a fatal AML according to the Bethesda guidelines[10] (median latency of 13, 23, and 26 days, respectively, for KMT2A::MLLT3+NRAS^{G12D}, FLT3^{ITD}, or FLT3^{N676K} as compared to 50 days for KMT2A::MLLT3-alone; p = 0.0004, p = 0.0002, and p = 0.0002, respectively). At leukemia development, most cells in the BM expressed both KMT2A::MLLT3 and the activating mutation (>77%, Supporting Information S1: Table 1). Mice had similar phenotypes with the AML cells expressing CD11b and Gr-1 and had a similar burden of leukemic granulocyte-macrophage-like progenitors (L-GMP). Leukemic cells gave rise to secondary malignancies identical to the primary disease in sublethally irradiated recipients, with reduced latency, with KMT2A::MLLT3+NRAS^{G12D} having the shortest latency. Mice were maintained in accordance with Lund University's ethical regulations. Five KMT2A-r infant acute leukemia patients with available whole genome sequencing data were included (Supporting Information S1: Table 2). Samples were obtained with informed consent. The murine and human studies were approved by the local Ethics committee of Lund University.

ATAC sequencing and analysis

Cells were thawed and purified by flow cytometry for viability and the murine cells were also enriched for cells that expressed GFP/mCherry, and 80 000 cells were then lysed in lysis buffer and used for the ATAC-seq protocol.[9] Nuclei were spun down and resuspended in the transposase reaction mix and purified using the MiniElute PCR Purification Kit (Qiagen). Fragments were pre-amplified as follows: 72°C for 5 min; 98°C for 30 s; 98°C for 10 s, 63°C for 30 s and 72°C for 1 min, 10 cycles. Libraries were purified using AMPure XP beads (Beckman Coulter). Agilent High Sensitivity DNA Assay (Agilent) and Qubit dsDNA High Sensitivity Assay Kit (Thermo Fisher Scientific) were used to assess quality. Sequencing was performed on the NextSeq. 500 (Illumina) using NextSeq. 500 high Output kit v2.0, 2 × 75 paired-end reads (200 million reads/sample). Adapters were trimmed using Trimmomatic (v0.39)[11] and subjected to quality control by fastQC (v0.12.1) [http://www.bioinformatics.babraham.ac.uk/projects/fastqc], aligned to mm9 or hg19 using bowtie2 (v2.5.1)[12] with parameters "-X 2000 --very-sensitive". Duplicates were removed using Picard (v2.6.0) MarkDuplicates [Picard Toolkit, http://broadinstitute.github.io/picard],[13] mitochondrial alignments, inappropriate alignments, alignments with mapping quality <Q30 were removed using Samtools (v1.9).[14] Filtered alignments were shifted +5 bp/−4 bp on the forward and reverse strand, respectively, using the ATACseqQC package (v1.8.5).[15] m16-11 had <30 million reads and was excluded (Supporting Information S1: Table 1).

Peaks were called using MACS2 (v2.1.0) callpeak command[16] with parameters "-f BAMPE -B --SPMR --keep-dup all -q 0.05". First, peaks were called individually; then, peaks for each genotype were merged using BEDTools (v2.26.0) intersect.[17] Only peaks present in at least 3/4 replicates (2/3 in KMT2A::MLLT3+NRAS^{G12D}) were kept. Then, all fifteen replicates were used to generate consensus peaks, and ENCODE blacklisted regions[18] were removed using BEDTools intersect. Read counts for consensus peaks were generated by BEDTools multicov, merged, and annotated using annotatePeaks.pl from HOMER.[19] BigWig files were generated using deepTools (v3.5.1)[20] bamCoverage command with parameters "--normalizeUsing CPM", and blacklisted regions were excluded.

Differential chromatin accessibility analysis

Differential accessible regions in the murine leukemias were determined by comparing all activating mutations to KMT2A::MLLT3-alone, as well as each activating mutation to KMT2A::MLLT3-alone using DESeq2 (v1.20.0)[21] with a fold change of ≥2 and Benjamini-Hochberg adjusted p < 0.05. When analyzing differential accessible regions (DARs) in normal hematopoietic mouse cells, each hematopoietic cell subpopulation was compared to hematopoietic stem cells as above. For the human data, the three patients with activating mutations were compared against the two patients lacking such mutations as above.

Hierarchical clustering and principal component analysis

The raw read count matrix was quantile normalized using the limma package,[22] then the top 75% of peaks with the highest read count were log2(quantile+0.5) transformed, and the Pearson correlation was calculated. Then, the Euclidean distance was computed, and hierarchical clustering was performed using the ward.D2 agglomeration method. For principal component analysis (PCA), the mouse and patient data were processed with respective selected normal cells (GSE162551, GSE143270 for normal mouse, and GSE122989, GSE74912 for normal human cells),[23–27] and batch effects were removed using the "sva" package (v3.30.1),[28] CPM normalized, log2(CPM+1) transformed, and subjected to PCA analysis using Qlucore Omics Explorer 3.9 (Qlucore, Lund, Sweden). For PCA analysis, variables were prefiltered by standard deviation(S/Smax) 0.3 and used to visualize the segregation of the normal cells.

cis-element and enrichment analysis

Each DAR was extended 500Kb from the peak middle toward both sides and intersected with promoters (TSS to upstream 2 kb) to generate raw DAR-target gene pairs. Only pairs with significantly differentially expressed genes (DEG) were kept as cis-element and target gene pairs. Genes were subjected to Metascape[29] for enrichment analysis with a significant threshold of EASE score (modified Fisher Exact) < 0.05.

TF binding motif analysis

TF binding motifs were analyzed using RGT HINT (v0.13.2).[30] Briefly, the motif sequences were scanned on all consensus peaks and DARs using "rgt-motifanalysis matching"; then, motifs on DARs were examined for enrichment against all consensus peaks using "rgt-motifanalysis enrichment." The footprints were called on DAR regions using "rgt-hint footprinting," and motifs overlapping footprints were obtained using "rgt-motifanalysis matching"; then, differential footprints were compared using "rgt-hint differential."

ChIP-seq and Hi-C analysis

ChIP-seq data for H3K27ac and H3K4me3 from murine KMT2A::MLLT3 AML (GSE143270)[24] and the RN2 cell line (GSE52277),[31] KMT2A-AFF1 pediatric ALL (GSE135026),[32] and THP-1 (GSE117864)[33] were downloaded and processed following a similar workflow as for the ATAC-seq. Briefly, clean reads were mapped to mm9 or hg19 using bowtie2,[12] deduplicated [Picard Toolkit, http://broadinstitute.github.io/picard],[13] low-quality alignments or mitochondrial reads were filtered out, and BigWig files were generated as above. Mouse Hi-C loops were obtained from the CH12-LX cell line (GSE63525; mm9),[34,35] normal HSPCs (GSE146669; mm10),[36] and normal hematopoietic cells (GSE152918; mm10);[37] the loops coordinates from mm10 were transformed to mm9 using LiftOver[38] and merged. Human Hi-C loops were obtained from THP-1 cells (PRJNA385337; hg19)[39,40] and merged.

Enhancer analysis

Mouse and human enhancers and enhancer–promoter interactions were downloaded from EnhancerAtlas,[41] and interactions from hematopoietic and leukemia cells were used and merged.

CAR design and viral production

The murine NKG2D-CAR was composed of a human CD8α signaling peptide followed by the extracellular domain of mouse NKG2D fused to the mouse CD8α hinge/transmembrane domain, mouse 4-1BB intracellular domain, and mouse CD3ζ intracellular domain. The mouse NKG2D-CAR was cloned into a retroviral pMSCV vector. The human NKG2D-CAR was composed of a human CD8α signaling peptide followed by the extracellular domain of human NKG2D or a variable binding domain targeting CD19 (clone FMC63) and fused to the human CD8α hinge/transmembrane domain, human 4-1BB intracellular domain, and the human CD3ζ intracellular domain. Human CARs were cloned into a modified pHR′ SIN:CSW vector containing an SFFV promoter. To determine expression, a T2A self-cleaving peptide preceding either an enhanced green fluorescent protein (eGFP) for the murine CAR or a blue fluorescent protein (mTagBFP2) for the human CAR was attached to the coding sequence. DNA fragments were assembled using in-fusion cloning (Takara Bio). To produce retroviral particles containing the CAR, Lenti-X 293 T cells (Takara Bio) were transfected with the transgene expression vector and the viral packaging plasmid pCL_Eco (Addgene) using Fugene HD (Promega) for the retroviral vectors and the viral packaging plasmid pMD2.G and pCMVdR8.91 (both from Addgene) for lentiviral vectors using TransIT-Lenti Transfection reagent (Mirus Bio LLC).

Engineering of mouse and human T cells

Primary mouse T cells were purified from a homogenized murine spleen using MojoSort™ Mouse CD3 T Cell Isolation Kit (Biolegend) and protocol followed by CD3/CD28 T cell activation with Mouse T-Activator anti-CD3/anti-CD28 Dynabeads (11452D; Life Technologies) for 24 h in mouse T cell media (mTCM) consisting of RPMI-1640 with L-glutamine (Thermo Scientific), 10% fetal bovine serum (FBS; Thermo Scientific), 100 units/mL Penicillin, 100 g/mL streptomycin (Thermo Scientific), 55 μM β-mercaptoethanol (Sigma-Aldrich), 0.1 mM non-essential amino acids (Sigma-Aldrich), 1 mM sodium pyruvate (Thermo Scientific), and 10 mM HEPES (Thermo Scientific) supplemented with 100 U/mL rhIL-2 (R&D Systems). Activated T cells were spinoculated on a retronectin-coated (Takara Bio) plate at 2000g, 32°C for 1 h. Dynabeads (Life Technologies) were removed after 24 h, and cells were used in functional assays 48 h after transduction.

Primary human T cells were isolated from peripheral blood from anonymous healthy blood donors (Blodcentralen) by Ficoll density gradient centrifugation and negative selection with MojoSort Human CD3 T cell Isolation Kit (Biolegend) and then cultured in human T cell medium (hTCM) consisting of AIM-V medium (Gibco) with 10% FBS, 10 mM HEPES (Thermo Fisher Scientific), 1× Sodium pyruvate, 100 U/mL penicillin, 100 μg/mL streptomycin, and 30 U/mL recombinant human IL-2 (R&D Systems). Twenty-four hours after thawing, T cells were stimulated with human T-activator CD3/CD28 Dynabeads™ (Thermo Fisher Scientific), and after 24 h of stimulation, cells were lentivirally transduced, as described.[42] For in vitro experiments, CAR T cells were sorted based on mTagBFP2 expression using (BD FACSAria Fusion) and used in downstream assays after 7–9 days of resting.

Co-culturing assays

Established cell lines from leukemic mice with KMT2A::MLLT3+ NRAS^{G12D} or KMT2A::MLLT3-alone were used (Supporting Information S1: Table 1).[7] Murine co-culturing assays were conducted by mixing CAR T cells or untraduced T-cells with mouse leukemic cell lines at an effector-to-target ratio (E:T) from 1:1 to 1:16, with a total of 50 000 cells (1:1) in a 96-well in biological triplicates for 48 h. Cells were maintained in mTCM media complemented with mIL3 (Peprotech). Mono-Mac-6 cells (ACC-124; DSMZ) were transduced with the following retroviral constructs MSCV-NRAS^{G12D}-IRES-eGFP and MSCV-NRAS^{WT}-IRES-eGFP.[7] Cells were cultured with RPMI-1640 with L-glutamine (Thermo Scientific), 10% FBS (Thermo Scientific), and 100 units/mL Penicillin and sorted to purity based on eGFP expression. Human CAR T cells and transduced Mono-Mac-6 were mixed at E:T of 2:1, 1:1, and 1:2, with a total of 20,000 target cells (2:1) and maintained in hTCM. Mixed cells were treated either with dimethyl sulfoxide, 2 mM, or 10 mM of LBH589 (MedChemExpress) for 24 h. Analysis was performed using flow cytometry as described below, and three independent experiments were performed.

Flow cytometry

Frozen murine BM cells and cell lines were thawed and stained with antibodies. Dead cells were excluded with Draq7 (Biostatus), and

analysis was performed using the FACS LSRFortesa (BD Biosciences) and FlowJo (FlowJo, LLC). FACS Aria Fusion (BD Biosciences) was used for sorting the target cells. The following antibodies were used H2-K1 (1:100, clone AF6-88.5, RUO, ref 742863) (BD Biosciences), H2-Db (1:100, clone REA932, ref 130-115-587) and PAN-RAE (1:100, clone REA723, ref 130-111-469) (Miltenyi Biotec), and RAE1∂ (1:50, clone Charlotte 1d.23, ref 133203), CD45.1 (1:200, clone A20, ref 10716), and CD3e (1:200, clone 17A2, ref 100236) (Biolegend). Recombinant Human NKG2D Fc Chimera Protein (1299-NK) (R&D Systems) was used in combination with APC anti-human IgG Fc recombinant (QA19A42 clone, 366906) (Biolegend) to detect NKG2D ligands. For a more detailed analysis of NKG2D ligands, human MICA/B (FAB13001P) and ULBP-1 (FAB1380P) (R&D Systems) were used. For immunophenotyping, samples were stained in 50 to 100 μL of phosphate-buffered saline supplemented with 2% FBS for 20 to 30 min at 4°C or 30 min at RT. Mono-Mac-6 cell stains were blocked with Human TruStain FcX (Biolegend).

Statistics and visualization

Statistical analysis was performed in R v3.5 if not specified, and flow cytometry analysis was conducted using Prism v10 (GraphPad). R packages ggplot2 (v3.1.0),[43] gplots (v3.1.3),[44] and pheatmap (v1.0.12)[45] were used for visualization. The PCA plots were created in Qlucore Omics Explorer 3.9 (Qlucore). Comparison between the expression of genes in two groups was done by two-sided Mann–Whitney U test, and the co-culturing assay was analyzed by a two-way analysis of variance.

RESULTS

Activating mutations affected cellular states

To determine the impact of activating mutations on the chromatin accessibility landscape of KMT2A-r leukemia, we studied the BM of 15 mice with AML driven by $KMT2A::MLLT3$-alone or $KMT2A::MLLT3+FLT3^{ITD}$, $KMT2A::MLLT3+FLT3^{N676K}$, or $KMT2A::MLLT3+NRAS^{G12D}$ at the disease end point (Figure 1A and Supporting Information S1: Table 1).[7] The leukemia cells expressed CD11b and Gr-1 and had a similar burden of leukemic granulocyte-macrophage like-progenitors (L-GMP), with the activating mutations accelerating disease (median latency of 13, 23, and 26 days, respectively, for $NRAS^{G12D}$, $FLT3^{ITD}$, and $FLT3^{N676K}$ as compared to 50 days for $KMT2A::MLLT3$-alone and are described in detail in Hyrenius-Wittsten et al.).[7] The presence of an activating mutation was associated with an increased number of accessible peaks with 22.7% (19 726/86 731) being exclusive to such leukemias (Supporting Information S1: Figure 1a,b). Further, the activating mutations changed the genomic distribution of accessible peaks, with a slightly higher fraction of accessible regions in introns and intergenic regions observed in $KMT2A::MLLT3$ with activating mutations, while a slightly higher fraction on promoters was observed in leukemia with $KMT2A::MLLT3$-alone (Figure 1B). To extend our results to human leukemia, five infants with KMT2A-r ALL ($n = 4$) or mixed phenotype leukemia (MPAL, $n = 1$), three of which carried activating mutations, were also studied (Figure 1A and Supporting Information S1: Tables 1 and 2). Infant leukemia with activating mutations had fewer accessible peaks as compared to leukemia lacking such mutations, but similar to the murine AML, they displayed genome-wide changes in the distribution of the peaks, showing a slightly higher fraction of peaks located in promoters and lower in introns and intergenic regions (Supporting Information S1: Figure 1c–f). Further, half of the peaks in the murine AMLs with activating mutations located to enhancers and reached 80% in the infant leukemias (Mann–Whitney U test, $p = 0.01945$) (Supporting Information S1: Table 3). Collectively,

suggesting that activating mutations cause global chromatin changes and open chromatin regions that often co-localize with enhancers.

Hierarchical clustering of the chromatin peaks showed that the mouse leukemias clustered based on their activating mutation and that $KMT2A::MLLT3+FLT3^{N676K}$ shared similarities with both $FLT3^{ITD}$ and $NRAS^{G12D}$ (Figure 1C). All leukemias exhibited similar peak profiles across KMT2A-r target genes (Hoxa9, Meis1, Mef2c, and Myc); however, some of these genes showed differential expression with e.g., Mef2c being highly expressed upon $NRAS^{G12D}$- and $FLT3^{N676K}$-mutations (Supporting Information S1: Figure 1g,h). To determine which normal hematopoietic developmental stage the murine leukemias resembled,[23,24] we next identified differentially accessible regions (DARs) for each hematopoietic cell subpopulation as compared to hematopoietic stem cells (HSCs) and then investigated the top 200 upregulated and 200 downregulated DARs with the lowest BH-adjusted p values from each hematopoietic subpopulation in the mouse leukemias (Figure 1D, Supporting Information S1: Figure 1i, Supporting Information S1: Tables 4 and 5). This showed that almost all these regions were more accessible in the presence of $NRAS^{G12D}$ or $FLT3^{N676K}$, as compared to in the presence of $FLT3^{ITD}$. To gain insights into associated gene expression changes, the genes nearest to these DARs were identified, and for example, Flt3, Emp1, Cttn, Cnn3, and Cd47 showed both altered expression and open chromatin upon $FLT3^{N676K}$- or $NRAS^{G12D}$- mutations with all but Cd47 also being among the closest genes to DARs in the murine AMLs (Figure 1E and Supporting Information S1: Figure 1j). Further, enrichment of processes associated with stemness were seen in all leukemias with activating mutations, with cell cycle and proliferation mainly being enriched in leukemia co-expressing $NRAS^{G12D}$ and $FLT3^{N676K}$ (Supporting Information S1: Figure 1k, Supporting Information S1: Table 6). Similar results were observed in infant leukemia with activating mutations which clustered closer to HSCs and MPPs, whereas leukemia lacking activating mutations clustered closer to common lymphoid progenitors (CLPs) (Figure 1F, Supporting Information S1: Table 4).[25,27]

Activating mutations remodeled the chromatin accessibility landscape

To decipher the impact of activating mutations on the global chromatin landscape and associated gene expression changes, DARs were identified. We first studied DARs that were common among activating mutations as compared to $KMT2A::MLLT3$-alone, identifying 4 391 DARs (FDR < 0.05) (Supporting Information S1: Figure 2a). Affected biological processes showed enrichment of for example, receptor protein tyrosine kinase signaling in leukemia with activating mutations (Supporting Information S1: Figure 2b). Next, DARs for each activating mutation were identified as compared to $KMT2A::MLLT3$-alone, identifying a total of 17 332 DARs ($KMT2A::MLLT3+NRAS^{G12D}$: 16 311, $KMT2A::MLLT3+FLT3^{N676K}$: 2 989, $KMT2A::MLLT3+FLT3^{ITD}$: 1 319, FDR < 0.05) (Figure 2A, Supporting Information S1: Figure 2c). Of identified DARs, >90% localized to introns/intergenic regions and around 40% overlapped with enhancers (Figure 2B, Supporting Information S1: Table 3). Similarly, in infant leukemia with activating mutations, 4 250 DARs were identified, with >90% localizing to introns/intergenic regions and 88% overlapped with enhancers (Figure 2C, Supporting Information S1: Figure 2d, Supporting Information S1: Table 3). This suggests that these distal regions might be cis-regulatory elements that drive distinct gene expression programs.

To determine the functional effect of open regions on gene expression, the DARs were integrated with corresponding gene expression data,[7] identifying a positive association between the openness of DARs and expression of the nearest genes both in mice and infant leukemia (Figure 2D,E). The genes nearest to the upregulated DARs in
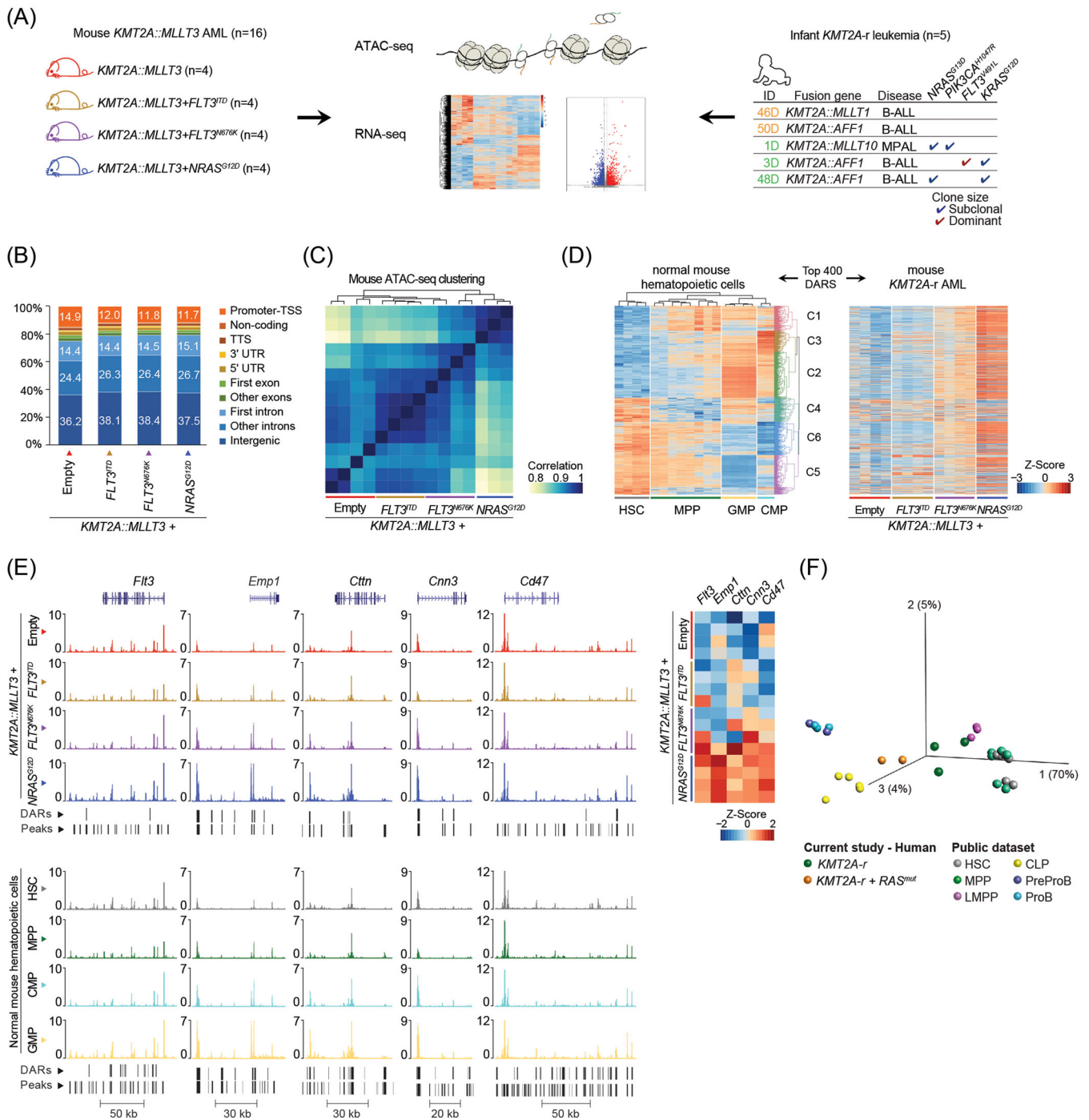
FIGURE 1 Activating mutations affected the cellular state. (A) Schematics of the experimental design, 16 mice with AML were studied by ATAC-sequencing and integrated with existing RNA-sequencing data (see also Hyrenius-Wittste et al., for details on the murine leukemias).[7] One *KMT2A::MLLT3+NRAS^G12D* mouse (m16-11) did not meet the Encode quality criteria for ATAC-seq data and was excluded (Supporting Information S1: Table 1). (B) Genomic annotation of peaks for each genotype of murine AML showing a lower fraction of peaks in promoters and a higher fraction in intergenic and intronic regions for murine *KMT2A::MLLT3* AML with activating mutations as compared to *KMT2A::MLLT3*-alone. (C) Pearson correlation of the open peaks in mouse leukemia samples showing clustering according to genotype. (D) left: chromatin accessibility comparison of normal mouse hematopoietic cells where the top 400 DARs (fold change ≥2, Benjamini-Hochberg adjusted *p* < 0.05) from pair-wise comparison of each subpopulation to hematopoietic stem cells (HSC) were used as input for hierarchical clustering. Right: the same top 400 DARs from each normal hematopoietic comparison in the same order when applied on the murine *KMT2A::MLLT3* leukemia samples. (E) Chromatin accessibility profiles (left) and transcript levels (right) of *Flt3*, *Emp1*, *Cttn*, *Cnn3*, and *Etv4* in the murine *KMT2A::MLLT3* AML and normal hematopoietic samples, respectively. DARs are indicated below and DARs outside of these plots can be found in Supporting Information S1: Tables 5 and 10. (F) PCA of the ATAC-data using infant *KMT2A*-r leukemia and normal hematopoietic cells, where the infant samples were projected into the PCA of the normal cells (GSE122989, GSE74912).[25–27]
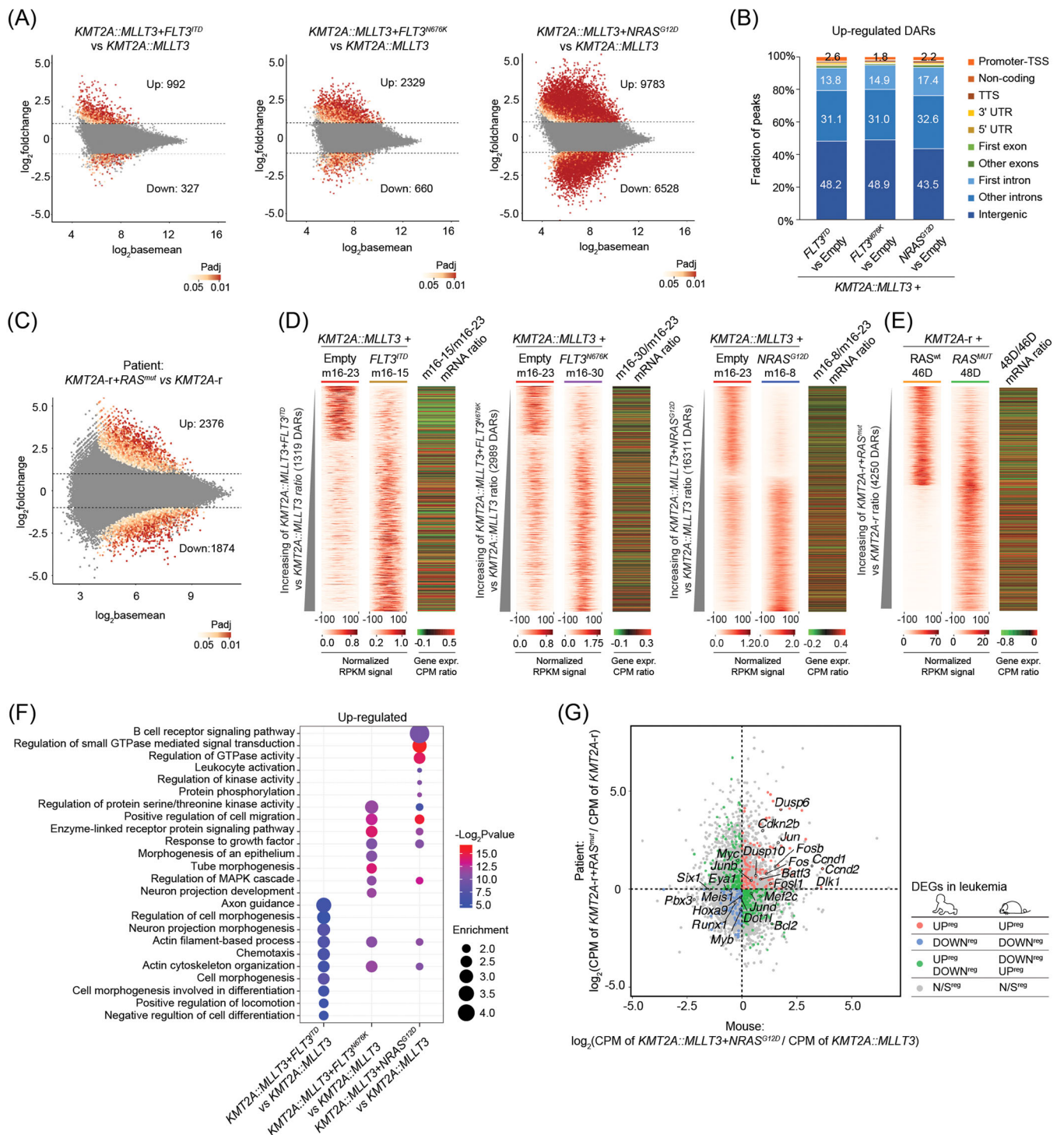
FIGURE 2 Activating mutations remodeled the chromatin accessibility landscape. **(A)** Number of DARs in *KMT2A::MLLT3*-driven AML carrying either of the activating mutations as compared to leukemia expressing *KMT2A::MLLT3*-alone. **(B)** Genomic annotation of up-regulated DARs in murine AML co-expressing *KMT2A::MLLT3* and either of the activating mutations. **(C)** Number of DARs in infant *KMT2A*-r leukemia with activating mutations as compared to those without. **(D)** Chromatin openness of murine *KMT2A::MLLT3* leukemia on DARs and the expression profiles of nearby genes for each mutation (*KMT2A::MLLT3+FLT3^{ITD}*: Pearson's cor = 0.23, p = 5.908e−14; *KMT2A::MLLT3+FLT3^{N676K}*: cor = 0.18, p < 2.2e−16; *KMT2A::MLLT3+NRAS^{G12D}*: cor = 0.23, p < 2.2e−16). **(E)** Chromatin openness of infant *KMT2A*-r leukemia on DARs and expression of nearby genes (Pearson's cor = 0.26, p < 2.2e−16). The DARs in **(D, E)** were ordered by increasing ratio of normalized RPKM signal in *KMT2A*-r with activating mutations to the signal in *KMT2A*-r alone. The color bar of ATAC-seq shows the normalized RPKM signal, signals on the DARs body as well as 100 bases up- and downstream of DARs are shown. The color bar of RNA-seq shows the gene expression ratio computed using CPM values. **(F)** Biological processes enriched among up-regulated DARs in murine leukemia co-expressing *KMT2A::MLLT3* and an activating mutation. **(G)** The overlap between nearby genes from DARs in murine *KMT2A::MLLT3+NRAS^{G12D}* and human homologs from nearby DARs in infant *KMT2A*-r+*RAS^{mut}* (hypergeometric test p = 1.02E−88 for upregulated and p = 1.47E−34 for downregulated genes). The three infant *KMT2A*-r+*RAS^{mut}* leukemias were combined and the two infant leukemias lacking an activating mutation were combined for this analysis. Dots in red: DEGs upregulated in both mouse and human leukemia; dots in blue: DEGs down-regulated in both mouse and human leukemia; dots in green: DEGs either upregulated in mice and down-regulated in human leukemia or downregulated in mouse and upregulated in human leukemia; dots in gray: genes nonsignificantly regulated. DEGs were identified using the corresponding RNA-seq data (fold change ≥1.5, Benjamini-Hochberg adjusted p < 0.05, 1236 upregulated and 845 downregulated genes).

KMT2A::MLLT3+FLT3^{N676K} or NRAS^{G12D} enriched for processes related to kinase activity and the MAPK-cascade, with similar processes affected in infant leukemia (Figure 2F, Supporting Information S1: Figure 2e,f). By contrast, KMT2A::MLLT3+FLT3^{ITD} enriched for processes linked to cell migration. Given that PI3K/RAS mutations activate MEK/ERK signaling, we investigated MEK/ERK-transcriptional output and negative feedback regulators.[46] We found that both were significantly enriched, with increased expression levels and chromatin accessibility of key genes in leukemia with NRAS^{G12D} or FLT3^{N676K} and in infant leukemia with activating mutations but not in the presence of FLT3^{ITD} (Supporting Information S1: Figure 2g–j, Supporting Information S1: Table 6). This enrichment was seen in our previous study,[7] and these results are extended by showing that the altered expression is connected to chromatin remodeling. Gene set enrichment analysis (GSEA)[47] also revealed enrichment of cell cycle and proliferation in leukemia with FLT3^{N676K} or NRAS^{G12D} and included high expression and open chromatin of Ccnd1, Ccnd2, and Cdkn2b (Supporting Information S1: Figure 3a,b, Supporting Information S1: Table 6). These results extended to the patient data with the infant leukemia cases harboring activating mutations displaying a higher expression of those genes as compared to cases lacking activating mutations (Supporting Information S1: Figure 3c,d). Combined, the DARs contribute to the transcriptomic differences observed upon activating mutations and suggest that the biological processes driven by FLT3^{ITD} were distinct from FLT3^{N676K} and NRAS^{G12D}.

We have previously demonstrated that the transcriptional profiles induced by activating mutations in human KMT2A-r leukemia were preserved in the mouse.[7] To examine if this extended to the chromatin landscape, the nearby genes from the patient DARs were transformed to mouse homologs and compared to the nearby genes from KMT2A::MLLT3+NRAS^{G12D} mice. We found that 40.5% of the upregulated and 28.8% of the downregulated genes overlapped and included negative regulators of MEK/ERK signaling (Dusp6, Dusp10), cell cycle genes (Ccnd1, Ccnd2), and the TFs (Jun, Fos, Fosb, Fosl1, Batf3) (Figure 2G, Supporting Information S1: Figure 3e–g), suggesting an overlap in how activating mutations promote leukemogenesis on a global level.

Distinct TF networks were activated

To determine if the activating mutations established TF networks that drive distinct gene expression programs, we performed TF binding motif enrichment and footprint profiling on the mutation-specific DARs.[30] This identified the motifs of Runx1/2 and Stat5a/Stat5b to be significantly enriched in FLT3^{ITD}-expressing leukemia, while the activator protein 1 (AP-1) family (Fos/Jund, Fosl1/Jun, Batf3/Jun) and its cofactors Smad2/Smad3 were enriched in FLT3^{N676K}- and NRAS^{G12D}-mutated AML (Figure 3A, Supporting Information S1: Table 7). Several, but not all of these TFs showed increased expression levels in the respective leukemias, and many motifs (Stat5a/Stat5b, Gata2, Fos, Jun, Fos/Jun, Fos/Junb, Jun/Junb, and Smad2/Smad3) also exhibited differential footprints (Figure 3B,C, Supporting Information S1: Figure 4a,b). Further, although both the motifs of Runx1 and Runx2 were enriched in FLT3^{ITD}-expressing leukemia, the high expression of Runx1 but not Runx2 suggests that the network is primarily driven by Runx1 (Figure 3B). To determine the binding signal of TFs on the motifs, we extracted the alignments on motifs and visualized them as in Figure 2D, showing that the respective motif signals were enhanced in KMT2A::MLLT3 co-expressing FLT3^{N676K} or NRAS^{G12D} while a weaker change was observed for FLT3^{ITD} (Figure 3D, Supporting Information S1: Figure 4c,d). Similarly, the AP-1 family and its cofactors were enriched among the upregulated DARs in infant leukemia with activating mutations and some also showed increased expression, differential footprints, and binding signals

(Figure 3E,F, Supporting Information S1: Figure 4e,f, Supporting Information S1: Table 8). This again demonstrates a biological overlap in how activating mutations promote leukemogenesis in human and mouse and that the TF networks established by FLT3^{ITD} were distinct from those established by FLT3^{N676K} and NRAS^{G12D}.

Activating mutations upregulated immune-associated regulatory networks

To gain insight into rewired transcriptional networks, we extracted regulatory regions by extending each mutation-specific DAR, 500Kb upstream and downstream from the peak middle, intersected with genome promoters to generate raw links between DARs and genes, and integrated that with DEGs (Supporting Information S1: Table 9). We obtained 837 DAR-DEG pairs in KMT2A::MLLT3+FLT3^{ITD}, 1430 pairs in KMT2A::MLLT3+FLT3^{N676K}, and 17134 pairs in KMT2A::MLLT3+NRAS^{G12D}, representing potential cis-regulatory elements and target gene links (Supporting Information S1: Table 10). Next, the DARs were combined and hierarchically clustered, forming five clusters, where clusters 1 and 3 mainly contained upregulated DARs-DEG pairs from NRAS^{G12D} and FLT3^{N676K} and clusters 2 and 4 upregulated pairs from FLT3^{ITD} (Figure 4A).

To determine the effect on downstream gene expression, we performed GO-analysis for each cluster, showing enrichment of immune-related processes in cluster 1 which contained a total of 9488 DARs (Figure 4A, Supporting Information S1: Figure 5a,b, Supporting Information S1: Table 11). This included MHC-class I genes involved in antigen presentation to T cells and in the regulation of immune-mediated cell killing by providing inhibitory signals to natural killer (NK) cells and macrophages. Several of these genes showed open chromatin and high gene expression including, for example, Raet1c/d, Klrd1, Klrg1, H2-K1, and H2-D1 (H2-Db) (Figure 4B, Supporting Information S1: Figure 5c). Flow cytometry confirmed Raet1a-d, H2-K1, and H2-D1 expression, in particular in NRAS^{G12D}-driven AML (Supporting Information S1: Figure 5d–h). Further, the AP-1 family motifs (Batf3, Fos/Jund, Fosl1/Jun, Jun) and cofactors Smad2/Smad3 were enriched in cluster 1 and enhanced signals of footprints and motif binding sites upon co-expression of NRAS^{G12D} or FLT3^{N676K} (Supporting Information S1: Figure 5i–k, Supporting Information S1: Table 12). In agreement, genes involved in immune processes (ARRB2, CEBPB, FCER1G, IFI30, IL6R, LYZ, ULBP2) displayed increased expression and open chromatin in infant leukemia with activating mutations (Figure 4C,D, Supporting Information S1: Figure 6a–c). Combined, oncogenic signaling by activating mutations caused chromatin remodeling that resulted in expression of immune regulatory genes.

Given that NRAS^{G12D}-driven AML expressed NKG2D (Klrk1) ligands, which are known mediators of immune surveillance,[48] we engineered an NKG2D-CAR to functionally validate immune recognition of KMT2A-r AML through NKG2D ligands. NKG2D-CAR T cells were incubated with murine AML expressing KMT2A::MLLT3-alone (n = 3) or KMT2A::MLLT3+NRAS^{G12D} (n = 4) at increasing E:T ratios, showing NKG2D-CAR T cell-mediated killing in a ratio-dependent manner (Figure 4E, Supporting Information S1: Figure 6d). Notably, leukemias expressing KMT2A::MLLT3-alone were also targeted and is likely explained by their low levels of Raet1 (Supporting Information S1: Figure 5g,h). In agreement, our gene expression data including normal mouse hematopoietic cells[7] showed elevated Raet1e expression in these leukemias and that NKG2D-ligand expression was minimal in normal cells (Supporting Information S1: Figure 5f). To link this finding to human leukemia, we utilized publicly available AML data sets (TCGA, BEAT, and Leukegene)[49–51] that showed similar expression of NKG2D ligands between KMT2A-r and KMT2A-wt samples (Supporting Information S1: Figure 6e). We next explored whether
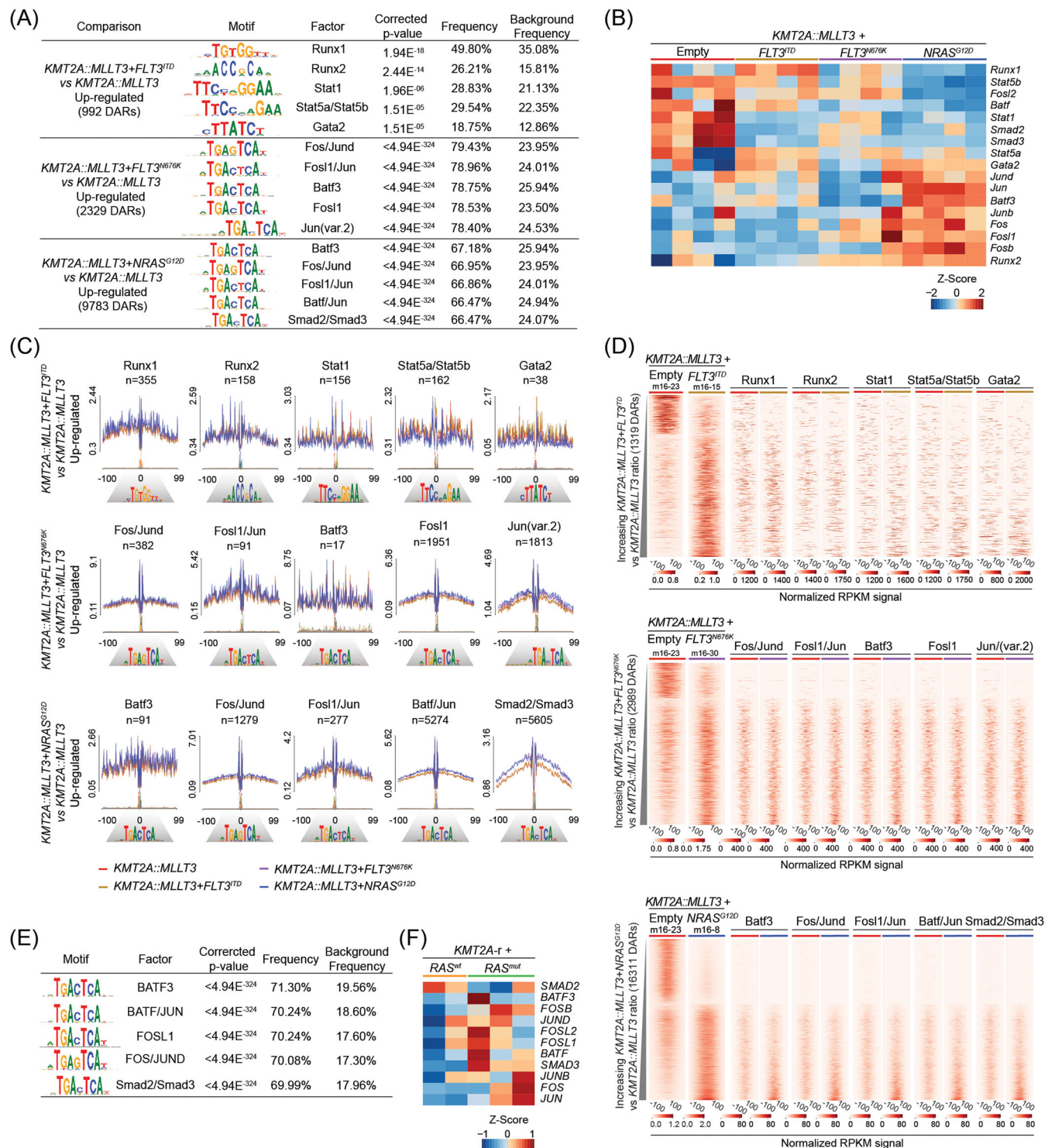
FIGURE 3 AP-1 transcription factors were activated by *FLT3*[N676K] and *NRAS*[G12D] in *KMT2A::MLLT3*-driven AML. **(A, B)** The most highly enriched motifs in the upregulated DARs in murine *KMT2A::MLLT3*-driven AML with activating mutations **(A)** and their transcription levels **(B)**. **(C)** Differential footprints of representative transcription factor motifs. The y-axis stands for the average ATAC-seq signal around the predicted transcription factor binding sites. The number of binding sites is shown on the top of each footprint portrait. **(D)** The binding signals of motifs on the DARs in each of the murine *KMT2A::MLLT3*-leukemias. The DARs were ordered by increasing ratio of normalized RPKM signal in *KMT2A::MLLT3* with activating mutations to the signal in *KMT2A::MLLT3* alone. The color bar shows the normalized RPKM signal. The signal on the DARs body as well as 100 bases up- and down-stream of DARs are shown. The motifs in panels **(A, C**, and **D)** are same. **(E, F)** The most highly enriched motifs in upregulated DARs in infant *KMT2A*-r leukemia with activating mutations **(E)** and their transcription levels **(F)**. For enriching motifs, the combined infant *KMT2A*-r leukemia with activating mutations (*n* = 3) and the combined infant leukemia with *KMT2A*-r alone (*n* = 2) were used.
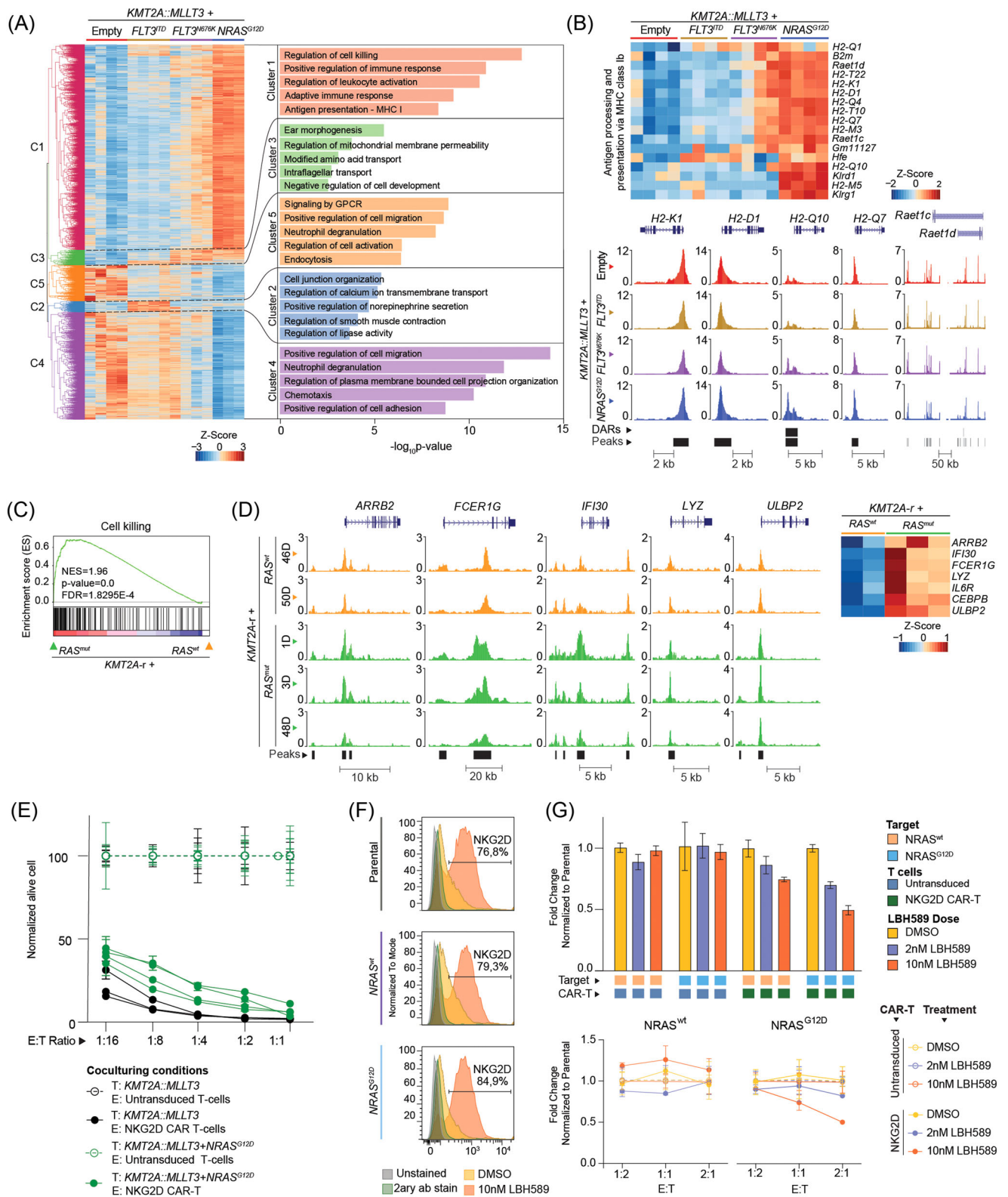
FIGURE 4 **Activating mutations promoted the expression of immune genes**. (A) Unsupervised hierarchical clustering of the combined DARs from murine *KMT2A::MLLT3* leukemia comparing each of the activating mutations to *KMT2A::MLLT3*-alone, and enriched biological process of the closest genes to the DARs. (B) Expression profiles of the GSEA leading-edge genes for one of the processes converging on immune cell regulation (top) and chromatin accessibility profiles of representative genes (bottom) in murine leukemia with or without activating mutations. (C, D) Immune gene sets enriched in infant *KMT2A*-r leukemia with activating mutations (C), chromatin accessibility profiles (D, left), and expression levels of representative genes (D, right). (E) Nkg2d-CAR T cells target *KMT2A*-r cells in a dose-responsive manner. (F) NKG2D expression in MM6 cells is induced upon treatment with LBH589 for 24 h irrespective of *NRAS* mutational status. (G) LBH589 allows MM6 cells to be targeted by NKG2D-CAR T cells and those expressing *NRAS*[G12D] are more efficiently targeted.

KMT2A-r AML cells could be pharmacologically sensitized to NKG2D-CAR T cells, as previously reported.[52] We therefore made use of the histone deacetylase inhibitor (HDACi) LBH589 (panobinostat)[52–54] that has been shown to upregulate NKG2D-ligand expression in AML.[55] Using the human NKG2D-ligand negative KMT2A::MLLT3 AML cell line Mono-Mac-6 (MM6), we could confirm that low dose LBH589 treatment led to a drastic upregulation of NKG2D-ligand levels regardless of NRAS mutational status (Figure 4F, Supporting Information S1: Figure 6f–h). Indeed, co-treatment of MM6 cells with LBH589 and NKG2D-CAR T cells enabled robust AML cell killing, and interestingly, the strongest effect was observed for MM6 cells expressing $NRAS^{G12D}$ (Figure 4G, Supporting Information S1: Figure 6i, Supporting Information S1: Table 13). Collectively, this indicates that KMT2A-r AML can be targeted by NKG2D-CAR T cells and that the expression levels of NKG2D ligands are further enforced by $NRAS^{G12D}$ and HDACi.

$FLT3^{ITD}$-associated chromatin and transcriptional networks

Our data suggested that $FLT3^{ITD}$ promoted KMT2A::MLLT3 leukemia differently as compared to $FLT3^{N676K}$ and $NRAS^{G12D}$, and the Nov/Ccn3 gene and the TF Socs2 were strongly activated in these leukemias (Figure 5A,B). Nov encodes a secreted protein associating with the extracellular matrix that promotes cell migration and is also a regulator of human cord blood stem and progenitor cells.[56,57] Moreover, the Mast cell protease (Mcpt) cluster genes (Mcpt1, Mcpt2, Mcpt4, Mcpt5/

Cma1, Mcpt8, Mcpt9) were markedly upregulated in $FLT3^{ITD}$ leukemia. Similar to Nov, these genes encode proteins in the extracellular matrix that normally are expressed by mast cells and have proteolytic activity.[58] We next explored their expression in normal mouse hematopoietic cell populations,[7] showing that their expression associated with specific immature hematopoietic cell populations, including Socs2 in the more immature cells and Ctsg and Gzmb in CMP/GMPs (Figure 5C).

The Mcpt cluster genes, as well as Granzyme (Gzm) cluster genes (Gzmb, Gzmc, Gzmd, Gzme, Gzmf, Gzmg, Gzmn) which were upregulated upon $NRAS^{G12D}$, are located within a 350Kb region, and ChIP-seq data[24,31] showed a strong H3K27ac signal in its center in the murine RN2 cell line containing $KMT2A::MLLT3 + Nras^{G12D}$ but not in murine AML driven by KMT2A::MLLT3 (Figure 5D, Supporting Information S1: Figure 7a). Further, enhancer coordinates[41] demonstrated the presence of an enhancer in this locus (chr14:56720909-56721677), and Hi-C data[34–37] and enhancer–promoter interactions[41] from normal hematopoietic and leukemic cells showed extensive cis-element interactions around this enhancer. Thus, an enhancer is likely turned on by the activating mutations that caused transcription of nearby genes through enhancer-promoter interactions, resulting in the expression of Mcpt-cluster genes upon $FLT3^{ITD}$ and of Gzm-cluster genes in the presence of $NRAS^{G12D}$. To link this finding to human leukemia, we utilized the human AML TCGA-data,[50] showing that both NOV and SOCS2 displayed a higher expression in $FLT3^{ITD}$-mutated AML as compared to those without such a mutation, but that CPT1B (corresponding to Mcpt1) did not (Figure 5E and not shown). Elevated NOV correlated with a lower overall survival irrespective of FLT3-mutational status (Figure 5F). Further,
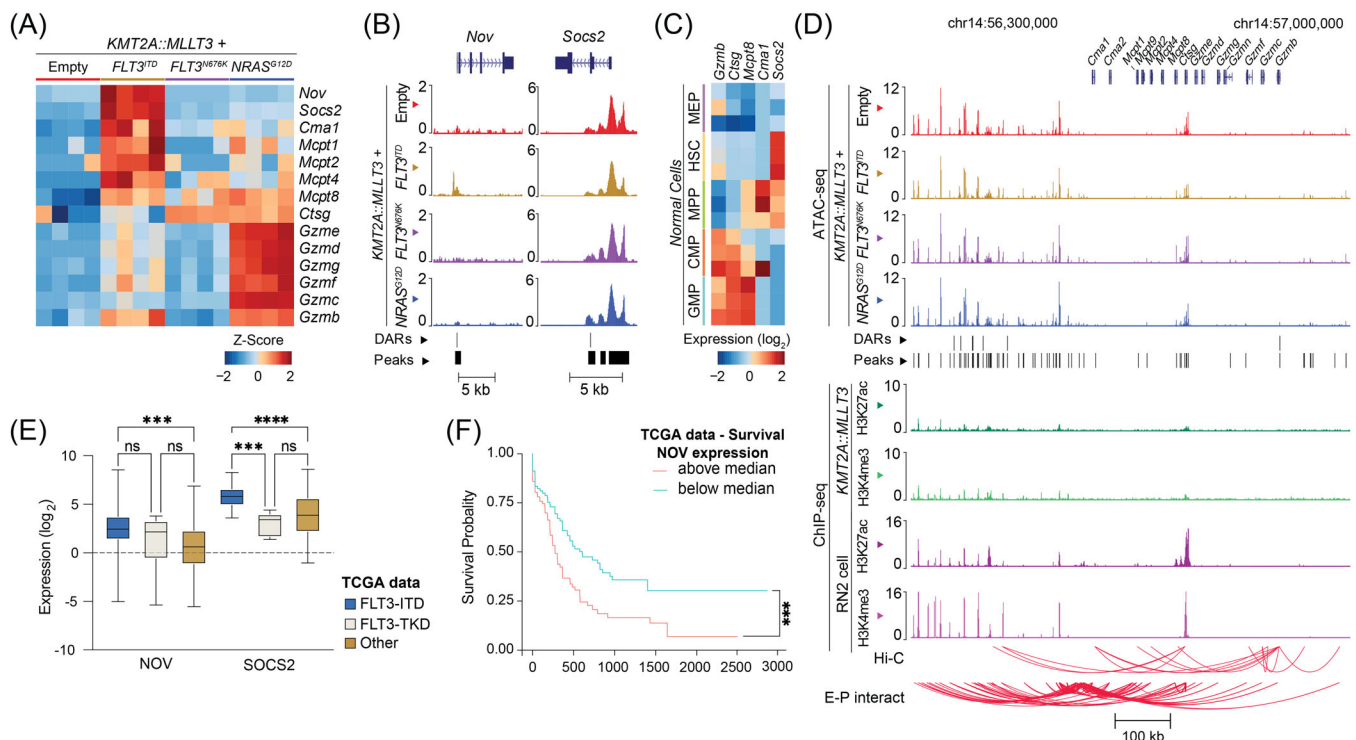

FIGURE 5 $FLT3^{ITD}$ induced mutation-specific gene expression profiles and chromatin accessibility landscape. (A) Heatmap showing the expression of selected genes in murine KMT2A::MLLT3 leukemia with or without activation mutations. (B) ATAC-seq tracks depicting chromatin accessibility at the Nov and Socs2 loci for the different genetic backgrounds mentioned in panel (A). Regions with DARs are highlighted. (C) Heatmap showing the expression of Gzmb, Cma1, Mcpt8, and Socs2 across various hematopoietic stem and progenitor cell populations from normal murine bone marrow. (D) ATAC-seq for the Gzmb, Cma1, Mcpt8 for a representative sample for each group, and public ChIP-seq data[24,31] that demonstrated an H3K27ac signal in the murine RN2 cell line containing $KMT2A::MLLT3+Nras^{G12D}$ but not in murine AML driven by KMT2A::MLLT3-alone. Enhancer coordinates[41] revealed an enhancer in this locus (chr14:56720909-56721677) and Hi-C data[34–37] and enhancer–promoter interactions[41] from normal hematopoietic and leukemic cells showed extensive cis-element interactions around this enhancer. (E) Box plots comparing NOV and SOCS2 expression levels in primary AML samples with different FLT3 mutations as compared to those without using the TCGA data. (F) Kaplan–Meier survival curves comparing overall survival in AML patients with survival above or below the median from the TCGA cohort based on NOV expression levels. Statistical significance is marked with ***$p < 0.001$ and ****$p < 0.001$.

GZMB did not associate with mutated *NRAS* in the TCGA data but with *TP53* mutations, suggesting that the high expression in our *NRAS*-mutated mice reflect their aggressiveness (Supporting Information S1: Figure 7b–d).

DISCUSSION

The mechanisms through which distinct activating mutations contribute to leukemia development remain poorly understood. Herein, we demonstrate that *FLT3*[N676K] and *NRAS*[G12D] induce chromatin alterations that promote AP-1-associated *cis*-regulation of transcriptional networks associated with stemness and immune cell regulation. The expression of immune cell ligands rendered the leukemia cells sensitive toward NKG2D-CAR T targeting. In contrast, *FLT3*[ITD] distinctly promotes leukemogenesis with Runx1 and Stat5a/b regulatory networks being activated that alter transcriptional programs linked to cell migration. These findings were extended and validated in *KMT2A*-r infant leukemia, suggesting a convergence in the mechanisms through which activating mutations facilitate leukemogenesis.

All activating mutations induced substantial chromatin remodeling in both mouse and human leukemia; however, the genomic distribution of identified peaks differed. In the mouse, most of the remodeling occurred in intronic and intergenic regions that overlapped with enhancers suggesting activation of *cis*-regulatory elements, with *NRAS*[G12D] having the largest impact. By contrast, in infant leukemia with activating mutations, primarily promoter regions were targeted. Further, in the murine AML, *FLT3*[N676K] shared more similarities with *NRAS*[G12D] than with *FLT3*[ITD], both at the chromatin and transcriptome level. Analysis of DARs from distinct normal hematopoietic cell subsets showed that especially *NRAS*[G12D] but also *FLT3*[N676K] had many of the same regions open. This is concordant with previous studies showing that *Nras* mutations enhance stemness.[59,60] The same shift toward an immature state was also seen in infant leukemia with activating mutations. Further, *Cd47*, a marker of leukemia stem cells and poor prognosis in human AML,[61] was highly expressed in AML with *NRAS*[G12D]. In human *KMT2A*-r AML, CD47 is lowly expressed;[62] thus, *Cd47* is likely activated by co-expression of *KMT2A::MLLT3*+*NRAS*[G12D].

Negative regulators of MEK/ERK-signaling[46] were induced by *NRAS*[G12D] or *FLT3*[N676K] but not to the same extent by *FLT3*[ITD], and these key genes are markers of MEK/ERK activation and likely independent of the co-expression of *KMT2A-MLLT3* and an activating mutation but rather linked to the activating mutation alone. Further, motif analysis identified the AP-1 TF family in both mouse and human *KMT2A*-r leukemia with *RAS*-mutations or *FLT3*[N676K] but not in the presence of *FLT3*[ITD]. The AP-1 family is a direct target of MAP kinases[63] and is not only activated in RAS/MAPK-mutated AML but also in *KMT2A*-r infant and childhood ALL.[8,36,64] This raises the possibility that the *KMT2A*-r-alone influences AP1-1-driven regulatory networks and that the activating mutations re-enforce this circuit.[65] This suggests that mutations in distinct domains of FLT3 have different downstream effects. In agreement, *FLT3*[ITD] causes a myeloproliferative disease, whereas tyrosine kinase domain (TKD) mutations cause lymphoid disease in mice.[66] Further, studies in 32D cells have shown signal transduction differences with TKD mutations failing to induce STAT5 target genes and repression of CEBPα.[67] Similarly, *FLT3*[N676K] does not activate Stat5 in BaF3 cells, nor in primary murine AML cells when co-expressed with *KMT2A::MLLT3* but do phosphorylate Akt and Erk.[7] Thus, different signaling mutations, even in the same gene, result in different chromatin accessibility and transcriptomic profiles.

Mechanistically, *FLT3*[ITD] was linked to Runx1 and Stat5a/Stat5b motifs, and these genes were also upregulated in *KMT2A::MLLT3*+*FLT3*[ITD] leukemia. *RUNX1* is highly expressed in human AML with *FLT3*[ITD] and *RUNX1* and *FLT3*[ITD] cooperate to induce AML in mice.[68,69] The most

significant processes in *FLT3*[ITD]-leukemias converged on cell migration, which was supported by chymase and mast cell protease genes that promote cell migration and metastasis.[70] These genes were likely activated by a nearby enhancer. Altered cell migration and invasion have also been described in human AML with *FLT3*[ITD].[71] Further, *Socs2* and *Nov* have been associated with oncogenic Flt3 signaling[36] and both showed high expression and chromatin openness in leukemia with *FLT3*[ITD] but not with *FLT3*[N676K]. Socs2 acts as a feedback inhibitor of FLT3[ITD] signaling; thus, *Socs2* is likely linked to activated Stat5a.[72] Further, NOV is induced after cytokine stimulation in HSC, directly through STAT5A/B,[73] linking both *Socs2* and *Nov* to *Stat5* and chronic FLT3[ITD]-signaling.

Genes associated with immune surveillance including NKG2D (*Klrk1*) ligands were enriched, particularly upon *NRAS*[G12D].[74] To validate immune recognition, we engineered an NKG2D-CAR T, demonstrating efficient killing of *KMT2A*-r cells. This immunological recognition could also be pharmacologically induced for an NKG2D ligand-negative *KMT2A*-r AML cell line, warranting further studies across different AML subtypes. Also, infant ALL with activating mutations displayed dysregulated immune signaling including expression and open chromatin of the UL16 binding protein 2 (*ULBP2*), an NKG2D-ligand. Although *ULBP2* activates T- and NK-cell-mediated killing upon NKG2D-binding, inappropriate shedding of NKG2D-ligands can instead promote immune escape.[75] Combined, our data not only demonstrates the potential utility of the NKG2D/NKG2D-ligand axis for targeting *KMT2A*-r leukemia but also suggests dysregulated immune surveillance upon activating mutations, warranting follow-up studies.

Here, we have started to delineate how various activating mutations affect the chromatin landscape and associated transcriptional networks in *KMT2A*-r acute leukemia. Our findings reveal that activating mutations impact chromatin architecture and activate transcriptional circuits that result in mutation-specific alterations in transcriptional programs. This included immune cell surveillance genes and our data suggests that *KMT2A*-r AML can be targeted by NKG2D-CAR T cells and that the expression level of NKG2D ligands can be enforced by *NRAS*[G12D] and pharmacologically by the HDACi LBH589. This underscores that the biological effect of activating mutation extends beyond mere proliferation and opens new therapeutic avenues for targeting the immunogenic phenotype of cells with activating mutations.

AUTHOR CONTRIBUTIONS

Anna K. Hagström-Andersson designed the study. Ton Falqués-Costa performed FACS analysis. Helena Sturesson prepared ATAC-seq libraries. Ton Falqués-Costa, Tina Ovlund, and Axel Hyrenius-Wittsten performed mouse CAR T cell experiments. Qirui Zhang, Ton Falqués-Costa, Mattias Pilheden, Vendela Rissler, Thoas Fioretos, Axel Hyrenius-Wittsten, and Anna K. Hagström-Andersson analyzed sequencing data. Qirui Zhang analyzed public omics data and developed scripts for omics data integrative analysis, functional enrichment, and motif analysis. Anders Castor, Hanne V. H. Marquart, and Birgitte Lausen provided patient material. Qirui Zhang, Ton Falqués-Costa, Axel Hyrenius-Wittsten, and Anna K. Hagström-Andersson wrote the manuscript. All authors approved the final version of the manuscript.

CONFLICT OF INTEREST STATEMENT

The authors declare no conflict of interest.

DATA AVAILABILITY STATEMENT

The data that support the findings of this study are openly available in Gene Expression Omnibus at https://0-www-ncbi-nlm-nih-gov.brum.beds.ac.uk/geo/, reference number GSE248468. The mouse RNA-seq (GSE106714) and ATAC-seq (GSE248468) are available in GEO and human data at DOI:10.17044/scilifelab.24260710. In-house scripts are available upon request.

ORCID

Ton Falqués-Costa http://orcid.org/0000-0002-5341-4472

Birgitte Lausen http://orcid.org/0000-0002-5306-0774

Anna K. Hagström-Andersson http://orcid.org/0000-0002-2904-1311

Axel Hyrenius-Wittsten http://orcid.org/0000-0002-1239-4954

SUPPORTING INFORMATION

Additional supporting information can be found in the online version of this article.

REFERENCES

1. Meyer C, Larghero P, Almeida Lopes B, et al. The KMT2A recombinome of acute leukemias in 2023. *Leukemia*. 2023;37(5):988-1005.
2. Pieters R, De Lorenzo P, Ancliffe P, et al. Outcome of infants younger than 1 year with acute lymphoblastic leukemia treated with the interfant-06 protocol: results from an international phase III randomized study. *J Clin Oncol*. 2019;37(25):2246-2256.
3. Hucks G, Rheingold SR. The journey to CAR T cell therapy: the pediatric and young adult experience with relapsed or refractory B-ALL. *Blood Cancer J*. 2019;9(2):10.
4. van der Sluis IM, de Lorenzo P, Kotecha RS, et al. Blinatumomab added to chemotherapy in infant lymphoblastic leukemia. *N Engl J Med*. 2023;388(17):1572-1581.
5. Agraz-Doblas A, Bueno C, Bashford-Rogers R, et al. Unraveling the cellular origin and clinical prognostic markers of infant B-cell acute lymphoblastic leukemia using genome-wide analysis. *Haematologica*. 2019;104(6):1176-1188.
6. Andersson AK, Ma J, Wang J, et al. The landscape of somatic mutations in infant MLL-rearranged acute lymphoblastic leukemias. *Nat Genet*. 2015;47(4):330-337.
7. Hyrenius-Wittsten A, Pilheden M, Sturesson H, et al. De novo activating mutations drive clonal evolution and enhance clonal fitness in KMT2A-rearranged leukemia. *Nat Commun*. 2018;9(1):1770.
8. Assi SA, Imperato MR, Coleman D, et al. Subtype-specific regulatory network rewiring in acute myeloid leukemia. *Nat Genet*. 2019;51(1):151-162.
9. Buenrostro JD, Giresi PG, Zaba LC, Chang HY, Greenleaf WJ. Transposition of native chromatin for fast and sensitive epigenomic profiling of open chromatin, DNA-binding proteins and nucleosome position. *Nat Methods*. 2013;10(12):1213-1218.
10. Kogan SC, Ward JM, Anver MR, et al. Bethesda proposals for classification of nonlymphoid hematopoietic neoplasms in mice. *Blood*. 2002;100(1):238-245.
11. Bolger AM, Lohse M, Usadel B. Trimmomatic: a flexible trimmer for Illumina sequence data. *Bioinformatics*. 2014;30(15):2114-2120.
12. Langmead B, Salzberg SL. Fast gapped-read alignment with Bowtie 2. *Nat Methods*. 2012;9(4):357-359.
13. toolkit P, Broad Institute. 2018.
14. Danecek P, Bonfield JK, Liddle J, et al. Twelve years of SAMtools and BCFtools. *Gigascience*. 2021;10(2):giab008.
15. Ou J, Liu H, Yu J, et al. ATACseqQC: a Bioconductor package for post-alignment quality assessment of ATAC-seq data. *BMC Genomics*. 2018;19(1):169.
16. Zhang Y, Liu T, Meyer CA, et al. Model-based analysis of ChIP-Seq (MACS). *Genome Biol*. 2008;9(9):137.
17. Quinlan AR, Hall IM. BEDTools: a flexible suite of utilities for comparing genomic features. *Bioinformatics (Oxford, England)*. 2010;26(6):841-842.
18. Amemiya HM, Kundaje A, Boyle AP. The ENCODE blacklist: identification of problematic regions of the genome. *Sci Rep*. 2019;9(1):9354.
19. Heinz S, Benner C, Spann N, et al. Simple combinations of lineage-determining transcription factors prime cis-regulatory elements required for macrophage and B cell identities. *Mol Cell*. 2010;38(4):576-589.
20. Ramirez F, Dundar F, Diehl S, Gruning BA, Manke T. deepTools: a flexible platform for exploring deep-sequencing data. *Nucleic Acids Res*. 2014;42(Web Server issue):W187-W191.
21. Love MI, Huber W, Anders S. Moderated estimation of fold change and dispersion for RNA-seq data with DESeq2. *Genome Biol*. 2014;15(12):550.
22. Ritchie ME, Phipson B, Wu D, et al. limma powers differential expression analyses for RNA-sequencing and microarray studies. *Nucleic Acids Res*. 2015;43(7):e47.
23. Itokawa N, Oshima M, Koide S, et al. Epigenetic traits inscribed in chromatin accessibility in aged hematopoietic stem cells. *Nat Commun*. 2022;13(1):2691.
24. Xiang G, Keller CA, Heuston E, et al. An integrative view of the regulatory and transcriptional landscapes in mouse hematopoiesis. *Genome Res*. 2020;30(3):472-484.
25. Corces MR, Buenrostro JD, Wu B, et al. Lineage-specific and single-cell chromatin accessibility charts human hematopoiesis and leukemia evolution. *Nat Genet*. 2016;48(10):1193-1203.
26. O'byrne S, Elliott N, Rice S, et al. Discovery of a CD10-negative B-progenitor in human fetal life identifies unique ontogeny-related developmental programs. *Blood*. 2019;134(13):1059-1071.
27. Bueno C, Barrera S, Bataller A, et al. CD34+CD19-CD22+ B-cell progenitors may underlie phenotypic escape in patients treated with CD19-directed therapies. *Blood*. 2022;140(1):38-44.
28. Leek JT, Johnson WE, Parker HS, Jaffe AE, Storey JD. The sva package for removing batch effects and other unwanted variation in high-throughput experiments. *Bioinformatics (Oxford, England)*. 2012;28(6):882-883.
29. Zhou Y, Zhou B, Pache L, et al. Metascape provides a biologist-oriented resource for the analysis of systems-level datasets. *Nat Commun*. 2019;10(1):1523.
30. Li Z, Schulz MH, Look T, Begemann M, Zenke M, Costa IG. Identification of transcription factor binding sites using ATAC-seq. *Genome Biol*. 2019;20(1):45.
31. Shi J, Whyte WA, Zepeda-Mendoza CJ, et al. Role of SWI/SNF in acute leukemia maintenance and enhancer-mediated Myc regulation. *Genes Dev*. 2013;27(24):2648-2662.
32. Godfrey L, Crump NT, O'byrne S, et al. H3K79me2/3 controls enhancer-promoter interactions and activation of the pan-cancer stem cell marker PROM1/CD133 in MLL-AF4 leukemia cells. *Leukemia*. 2021;35(1):90-106.
33. Godfrey L, Crump NT, Thorne R, et al. DOT1L inhibition reveals a distinct subset of enhancers dependent on H3K79 methylation. *Nat Commun*. 2019;10(1):2803.
34. Rao SS, Huntley MH, Durand NC, et al. A 3D map of the human genome at kilobase resolution reveals principles of chromatin looping. *Cell*. 2014;159(7):1665-1680.
35. Sanborn AL, Rao SS, Huang SC, et al. Chromatin extrusion explains key features of loop and domain formation in wild-type and engineered genomes. *Proc Natl Acad Sci USA*. 2015;112(47):6456-6465.

36. Yun H, Narayan N, Vohra S, et al. Mutational synergy during leukemia induction remodels chromatin accessibility, histone modifications and three-dimensional DNA topology to alter gene expression. *Nature Genet*. 2021;53(10):1443-1455.

37. Zhang C, Xu Z, Yang S, et al. tagHi-C reveals 3D chromatin architecture dynamics during mouse hematopoiesis. *Cell Rep*. 2020;32(13):108206.

38. Hinrichs AS, Karolchik D, Baertsch R, et al. The UCSC genome browser database: update 2006. *Nucleic Acids Res*. 2006;34(Database issue):D590-8.

39. Liu Y, Li H, Czajkowsky DM, Shao Z. Monocytic THP-1 cells diverge significantly from their primary counterparts: a comparative examination of the chromosomal conformations and transcriptomes. *Hereditas*. 2021;158(1):43.

40. Phanstiel DH, Van Bortle K, Spacek D, et al. Static and dynamic DNA loops form AP-1-bound activation hubs during macrophage development. *Mol Cell*. 2017;67(6):1037-1048.

41. Gao T, Qian J. EnhancerAtlas 2.0: an updated resource with enhancer annotation in 586 tissue/cell types across nine species. *Nucleic Acids Res*. 2020;48(D1):D58-D64.

42. Hyrenius-Wittsten A, Su Y, Park M, et al. SynNotch CAR circuits enhance solid tumor recognition and promote persistent antitumor activity in mouse models. *Sci Transl Med*. 2021;13(591):eabd8836.

43. Wickham H. *ggplot2: Elegant Graphics for Data Analysis*. Springer-Verlag; 2016.

44. Warnes G, Bolker B, Bonebakker L, et al. gplots: Various R programming tools for plotting data. 2005.

45. Kolde R pheatmap: Pretty Heatmaps. R package version 1.0. 12. 2019.

46. Pratilas CA, Taylor BS, Ye Q, et al. (V600E)BRAF is associated with disabled feedback inhibition of RAF-MEK signaling and elevated transcriptional output of the pathway. *Proc Natl Acad Sci USA*. 2009;106(11):4519-4524.

47. Subramanian A, Tamayo P, Mootha VK, et al. Gene set enrichment analysis: a knowledge-based approach for interpreting genome-wide expression profiles. *Proc Natl Acad Sci USA*. 2005;102(43):15545-15550.

48. Dhatchinamoorthy K, Colbert JD, Rock KL. Cancer immune evasion through loss of MHC Class I antigen presentation. *Front Immunol*. 2021;12:636568.

49. Bagger FO, Sasivarevic D, Sohi SH, et al. BloodSpot: a database of gene expression profiles and transcriptional programs for healthy and malignant haematopoiesis. *Nucleic Acids Res*. 2016;44(D1):917-924.

50. Cancer Genome Atlas Research N, Ley TJ, Miller C, et al. Genomic and epigenomic landscapes of adult de novo acute myeloid leukemia. *N Engl J Med*. 2013;368(22):2059-2074.

51. Tyner JW, Tognon CE, Bottomly D, et al. Functional genomic landscape of acute myeloid leukaemia. *Nature*. 2018;562(7728):526-531.

52. Driouk L, Gicobi JK, Kamihara Y, et al. Chimeric antigen receptor T cells targeting NKG2D-ligands show robust efficacy against acute myeloid leukemia and T-cell acute lymphoblastic leukemia. *Front Immunol*. 2020;11:580328.

53. Diermayr S, Himmelreich H, Durovic B, et al. NKG2D ligand expression in AML increases in response to HDAC inhibitor valproic acid and contributes to allorecognition by NK-cell lines with single KIR-HLA class I specificities. *Blood*. 2008;111(3):1428-1436.

54. Poggi A, Catellani S, Garuti A, Pierri I, Gobbi M, Zocchi MR. Effective in vivo induction of NKG2D ligands in acute myeloid leukaemias by all-trans-retinoic acid or sodium valproate. *Leukemia*. 2009;23(4):641-648.

55. Sauer M, Schuldner M, Hoffmann N, et al. CBP/p300 acetyl-transferases regulate the expression of NKG2D ligands on tumor cells. *Oncogene*. 2017;36(7):933-941.

56. Gupta R, Hong D, Iborra F, Sarno S, Enver T. NOV (CCN3) functions as a regulator of human hematopoietic stem or progenitor cells. *Science*. 2007;316(5824):590-593.

57. Liang T, Shen L, Ji Y, Jia L, Dou Y, Guo L. NOV/CCN3 promotes cell migration and invasion in intrahepatic cholangiocarcinoma via miR-92a-3p. *Genes*. 2021;12(11):1659.

58. Berlin F, Mogren S, Tutzauer J, Andersson CK. Mast cell proteases tryptase and chymase induce migratory and morphological alterations in bronchial epithelial cells. *Int J Mol Sci*. 2021;22(10):5250.

59. Li Q, Bohin N, Wen T, et al. Oncogenic Nras has bimodal effects on stem cells that sustainably increase competitiveness. *Nature*. 2013;504(7478):143-147.

60. Sachs Z, LaRue RS, Nguyen HT, et al. NRASG12V oncogene facilitates self-renewal in a murine model of acute myelogenous leukemia. *Blood*. 2014;124(22):3274-3283.

61. Majeti R, Chao MP, Alizadeh AA, et al. CD47 is an adverse prognostic factor and therapeutic antibody target on human acute myeloid leukemia stem cells. *Cell*. 2009;138(2):286-299.

62. Marra A, Akarca AU, Martino G, et al. CD47 expression in acute myeloid leukemia varies according to genotype. *Haematologica*. 2023;108:3491-3495.

63. Smith ER, Smedberg JL, Rula ME, Xu XX. Regulation of Ras-MAPK pathway mitogenic activity by restricting nuclear entry of activated MAPK in endoderm differentiation of embryonic carcinoma and stem cells. *J Cell Biol*. 2004;164(5):689-699.

64. Barnett KR, Mobley RJ, Diedrich JD, et al. Epigenomic mapping reveals distinct B cell acute lymphoblastic leukemia chromatin architectures and regulators. *eCollection*. 2023;3(12):100442. https://doi.org/10.1016/j.xgen.2023.100442

65. Tejedor JR, Bueno C, Vinyoles M, et al. Integrative methylome-transcriptome analysis unravels cancer cell vulnerabilities in infant MLL-rearranged B cell acute lymphoblastic leukemia. *J Clin Invest*. 2021;131(13):e138833.

66. Grundler R, Miething C, Thiede C, Peschel C, Duyster J. FLT3-ITD and tyrosine kinase domain mutants induce 2 distinct phenotypes in a murine bone marrow transplantation model. *Blood*. 2005;105(12):4792-4799.

67. Choudhary C, Schwäble J, Brandts C, et al. AML-associated Flt3 kinase domain mutations show signal transduction differences compared with Flt3 ITD mutations. *Blood*. 2005;106(1):265-273.

68. Behrens K, Maul K, Tekin N, et al. RUNX1 cooperates with FLT3-ITD to induce leukemia. *J Exp Med*. 2017;214(3):737-752.

69. Cauchy P, James SR, Zacarias-Cabeza J, et al. Chronic FLT3-ITD signaling in acute myeloid leukemia is connected to a specific chromatin signature. *Cell Rep*. 2015;12(5):821-836.

70. Pejler G, Rönnberg E, Waern I, Wernersson S. Mast cell proteases: multifaceted regulators of inflammatory disease. *Blood*. 2010;115(24):4981-4990.

71. Ortlepp C, Steudel C, Heiderich C, et al. Autotaxin is expressed in FLT3-ITD positive acute myeloid leukemia and hematopoietic stem cells and promotes cell migration and proliferation. *Exp Hematol*. 2013;41(5):444-461.

72. Kazi JU, Rönnstrand L. Suppressor of cytokine signaling 2 (SOCS2) associates with FLT3 and negatively regulates downstream signaling. *Mol Oncol*. 2013;7(3):693-703.

73. Kimura 木村丹香子 A, Martin C, Robinson GW, et al. The gene encoding the hematopoietic stem cell regulator CCN3/NOV is under direct cytokine control through the transcription factors STAT5A/B. *J Biol Chem*. 2010;285(43):32704-32709.

74. Liu XV, Ho SS, Tan JJ, Kamran N, Gasser S. Ras activation induces expression of Raet1 family NK receptor ligands. *J Immunol*. 2012;189(4):1826-1834.

75. Groh V, Wu J, Yee C, Spies T. Tumour-derived soluble MIC ligands impair expression of NKG2D and T-cell activation. *Nature*. 2002;419(6908):734-738.